FEBS Letters 585 (2011) 447–451

FEBS Letters

journal homepage: www.FEBSLetters.org

Structure of the *E*-1-hydroxy-2-methyl-but-2-enyl-4-diphosphate synthase (GcpE) from *Thermus thermophilus*

Ingo Rekittke [a], Tsuyoshi Nonaka [b], Jochen Wiesner [a], Ulrike Demmer [b], Eberhard Warkentin [b], Hassan Jomaa [a,*], Ulrich Ermler [b,*]

[a] Institut für Klinische Immunologie und Transfusionsmedizin, Justus-Liebig-Universität Giessen, Langhansstraße 7, 35392 Giessen, Germany
[b] Max-Planck-Institut für Biophysik, Max-von-Laue-Straße 3, D-60438 Frankfurt am Main, Germany

ARTICLE INFO

Article history:
Received 9 November 2010
Revised 6 December 2010
Accepted 8 December 2010
Available online 15 December 2010

Edited by Richard Cogdell

Keywords:
Non-mevalonate pathway
E-1-hydroxy-2-methyl-but-2-enyl-4-diphosphate synthase
Iron–sulfur cluster
X-ray structure
Drug design

ABSTRACT

Isoprenoids are biosynthesized via the mevalonate or the 2-*C*-methyl-D-erythritol-4-phosphate (MEP) pathways the latter being used by most pathogenic bacteria, some parasitic protozoa, plant plastids, but not by animals. We determined the X-ray structure of the homodimeric [4Fe–4S] cluster carrying *E*-1-hydroxy-2-methyl-but-2-enyl-4-diphosphate synthase (GcpE) of *Thermus thermophilus* which catalyzes the penultimate reaction of the MEP pathway and is therefore an attractive target for drug development. The [4Fe–4S] cluster ligated to three cysteines and one glutamate is encapsulated at the intersubunit interface. The substrate binding site lies in front of an $(\alpha\beta)_8$ barrel. The great [4Fe–4S] cluster-substrate distance implicates large-scale domain rearrangements during the reaction cycle.

Structured summary:
gcpE binds to **gcpE** by x-ray crystallography (View interaction)

1. Introduction

Isoprenoids such as dolichol, quinones, carotenoids, vitamins and sterols, are synthesised from isopentenyl diphosphate and its isomer, dimethylallyl diphosphate by two completely different biosynthetic pathways dependent on the organism. Animals, fungi, archaea and some bacteria, use the well-known mevalonate pathway, the vast majority of bacteria and some parasitic protozoa of the phylum apicomplexa, the 2-*C*-methyl-D-erythritol-4-phosphate (MEP) pathway [also known as the 1-deoxy-D-xylulose-5-phosphate, or non-mevalonate pathway] (Fig. 1) [1–3]. In plants, the mevalonate pathway is operative in the cytosol, while the MEP pathway functions inside the plastids. Since the MEP pathway is not used by humans, it represents an attractive target for the development of new antimicrobial and herbicidal compounds [4,5].

In the penultimate step of the MEP pathway, 2-*C*-methyl-D-erythritol-2,4-cyclo-diphosphate (MEcPP) is converted to *E*-1-hydroxy-2-methyl-but-2-enyl-4-diphosphate (HMBPP) by the Fe/S cluster carrying enzyme HMBPP synthase termed *E*-1-hydroxy-2-methyl-but-2-enyl-4-diphosphate synthase (GcpE) or IspG (Fig. 1) [6–9]. The catalyzed C=C double bond formation is mechanistically difficult because two basic groups are eliminated (one dissociation implies a ring opening) and the lacking two electrons are supplied one by one by a protein-bound Fe/S cluster. Diverse mechanistic scenarios for the GcpE reaction were postulated involving cations, radicals and anions and recently Fe/S cluster intermediates including iron–carbon species [7,9–13]. GcpE is a homodimeric enzyme with a molecular mass of about 40–45 kDa per monomer [7,10]. Based on Mössbauer and EPR spectroscopic data, the highly dioxygen sensitive Fe/S cluster was identified as a [4Fe–4S] cluster type ligated to three cysteine residues [14,15]. The protein-bound [4Fe–4S] cluster is reduced in vivo by flavodoxin or ferredoxin and NADPH depending on the organism [16] and in vitro by 5-deazaflavin and dithionite [15]. The reaction has been kinetically characterized for GcpE from several organisms [17]. For example, the specific activity of *Thermus thermophilus* GcpE was 0.6 μmol min^{-1} mg^{-1} at pH 7.5, the k_{cat} value 0.4 s^{-1} and the K_m value of HMBPP 0.42 mM [7].

For understanding this fascinating reaction on an atomic basis and for opening a perspective for rational drug design, we solved

Abbreviations: GcpE, *E*-1-hydroxy-2-methyl-but-2-enyl-4-diphosphate synthase; MEP, 2-*C*-methyl-D-erythritol-4-phosphate; MEcPP, 2-*C*-methyl-D-erythritol-2,4-cyclo-diphosphate; HMBPP, *E*-1-hydroxy-2-methyl-but-2-enyl-4-diphosphate

* Correspondence authors. Fax: +49 641 9941509 (H. Jomaa); +49 6963031002 (U. Ermler).
E-mail addresses: hassan.jomaa@uniklinikum-giessen.de (H. Jomaa), ulrich.ermler@biophys.mpg.de (U. Ermler).

0014-5793/$36.00
doi:10.1016/j.febslet.2010.12.012

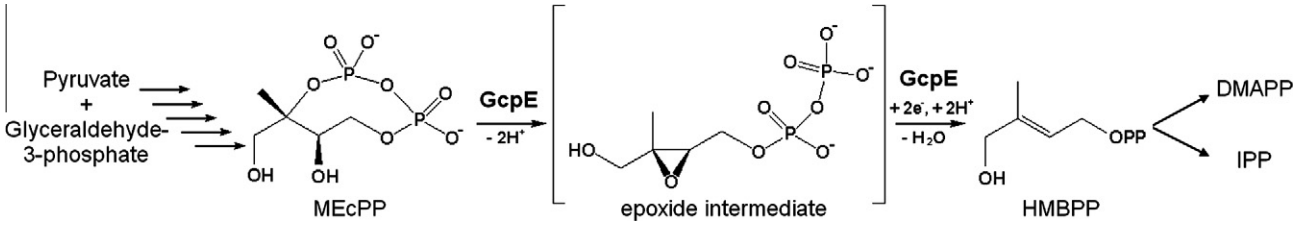

Fig. 1. MEP pathway and the reaction of GcpE. Isopentenyl diphosphate (IPP) and its isomer, dimethylallyl diphosphate (DMAPP) are the precursors of isoprenoid biosynthesis.

the structure of GcpE from *T. thermophilus* at 2.5 Å resolution. We describe the architecture of the enzyme as well as the binding mode of the [4Fe–4S] cluster and discuss the putative substrate binding site and mechanistic aspects. During writing of the manuscript, the GcpE structure of *Aquifex aeolicus* was reported by Lee et al. [18].

2. Materials and methods

2.1. Enzyme production

All experiments were carried out under oxygen exclusion. TOP 10 *Escherichia coli* cells (Invitrogen) were transformed with the PQETtGcpE vector containing untagged GcpE and grown in LB-broth (Roth) supplemented with 150 μg ml^{-1} ampicillin and 300 μM $FeCl_3$ at 37 °C [7]. The cells were harvested by centrifugation (17700×*g*, 15 min, 4 °C) and stored at −30 °C until use. The cell pellet (40 g) was resuspended in 400 ml 30 mM Tris–HCl (pH 7.5) and lysed by ultrasonic treatment at 0 °C. Purification was performed using a DEAE, a Source 15 Q and a Superdex 200 column as described in Supplementary data. GcpE was stored at a concentration of ca. 12 mg ml^{-1}, in 30 mM Tris–HCl, pH 7.5 and 150 mM NaCl for crystallization.

2.2. Crystallization and X-ray structure analysis

Crystallization was performed at 18 °C using the sitting drop vapour diffusion method. Best crystals grew by mixing 1.0 μl enzyme solution and 1.0 μl reservoir solution composed of 30% (v/v) MPD and 20% (v/v) ethanol. Data were collected at the Swiss-Light source beamline PXII and processed with XDS [19]. Phase determination is described in Supplement. The structure was refined using REFMAC [20]. Crystal parameters, data collection and refinement statistics are listed in Supplementary Table 1. Figs. 2–4 were prepared with MOLSCRIPT [21] and CHIMERA [22]. The atomic coordinates and structure factors of GcpE have been deposited in the Protein Data Bank, www.pdb.org with ID codes 2y0f, respectively.

3. Results and discussion

3.1. Overall architecture of the enzyme

Recombinant untagged GcpE from *T. thermophilus* was crystallized under strictly anaerobic conditions and its structure determined with the multiple anomalous dispersion method based on the irons of the Fe/S cluster (see Supplementary Table 1). The final R/R_{free} factors are 20.0%/26.3% at 2.5 Å resolution. The structure is relatively mobile resulting in temperature factors of the four monomers in the asymmetric unit of about 75, 85, 97, 102 Å^2, respectively.

Architecturally, each GcpE monomer of the homodimer (residues marked A and B) is composed of two domains (Fig. 2A + Supplementary Fig. 1). The N-terminal domain (A4:A285) essentially consists of the well-known TIM barrel fold which revealed – according to Dali [23] – the highest structural relationship to dihydropteroate synthase (3h24-A) with an rms deviation of 2.7 Å (84% of the C_α atoms used). Three noteworthy differences exist between GcpE and the canonical $(\beta\alpha)_8$ barrel including a β-hairpin (A7:A22) forming the N-terminal bottom of the β-barrel, a break of helix 3 into two small helices (perhaps for adjusting strand 4) and a helix-loop-helix protrusion after strand 5 (Fig. 2 + Supplementary Fig. 1). The exposed protrusion is mainly fixed by interactions to the counter subunit (see below) but also to the β-barrel core by the loop after strand 6 and, in particular, by the stretch following the shortened strand 4. The β-barrel interior adopts a funnel-like shape. The funnel is locked by side chains of the parallel strands at the end of the narrow segment before it becomes wider (see below). The C-terminal domain (A291–A404) consists of an open αβ structure (Fig. 2A + Supplementary Fig. 1). Its fold corresponds to one sulfite reductase domain the highest relationship being found to the *Desulfovibrio vulgaris* enzyme (2v4j-B) with an rms deviation of 3.0 Å (27% of the C_α atoms used). The mixed five-stranded β-sheet is flanked by two long helices on one side and a short helix distorted by ProA348 on the other. The latter side also serves as primary binding site for the [4Fe–4S] cluster.

The two globular domains are connected by a highly solvent-exposed linker of about five residues (A286–A290) (Fig. 2). Solely, these residues form a few non-covalent, mostly short-range interactions between the two domains. Therefore, the observed orientation between the two domains is essentially determined by interactions with the counter subunit of the GcpE homodimer (Fig. 2B) [7]. (The structural data are even compatible with a homotetrameric state.) The monomers of the dimer are oriented to each other in a head-to-tail arrangement forming three contact areas. In the two peripheral interfaces, each burying a surface area of ca. 460 Å^2, the helix-loop-helix protrusion of one subunit faces strand 1′ and helix 2′ of the counter subunit and vice versa. The third extended interface with a surface area of ca. 1010 Å^2 is found between the central TIM barrel domains involving helices 6 (its N-terminal end), 7 and 8 of both subunits (Fig. 2B). Although the GcpE dimer conveys a rather fragile impression, the related domain-domain arrangements in the four monomers of the asymmetric unit indicate sufficient rigidity and stability.

3.2. Binding mode of the Fe/S cluster

The electron density profile at the position of the Fe/S cluster clearly argues for a [4Fe–4S] cluster in agreement with EPR spectroscopic data [15]. The [4Fe–4S] cluster is highly occupied, as its temperature factor (69 Å^2) is only moderately higher than that of the polypeptide environment.

The [4Fe–4S] cluster of each monomer is embedded into the crevice formed by strands 1′ and 2′ and the following loops (directed towards different sides of the β-sheet plane) capped by the helix-loop-helix protrusion of the respective counter subunit (Figs. 2 and 3). It is essentially shielded from bulk solvent despite the

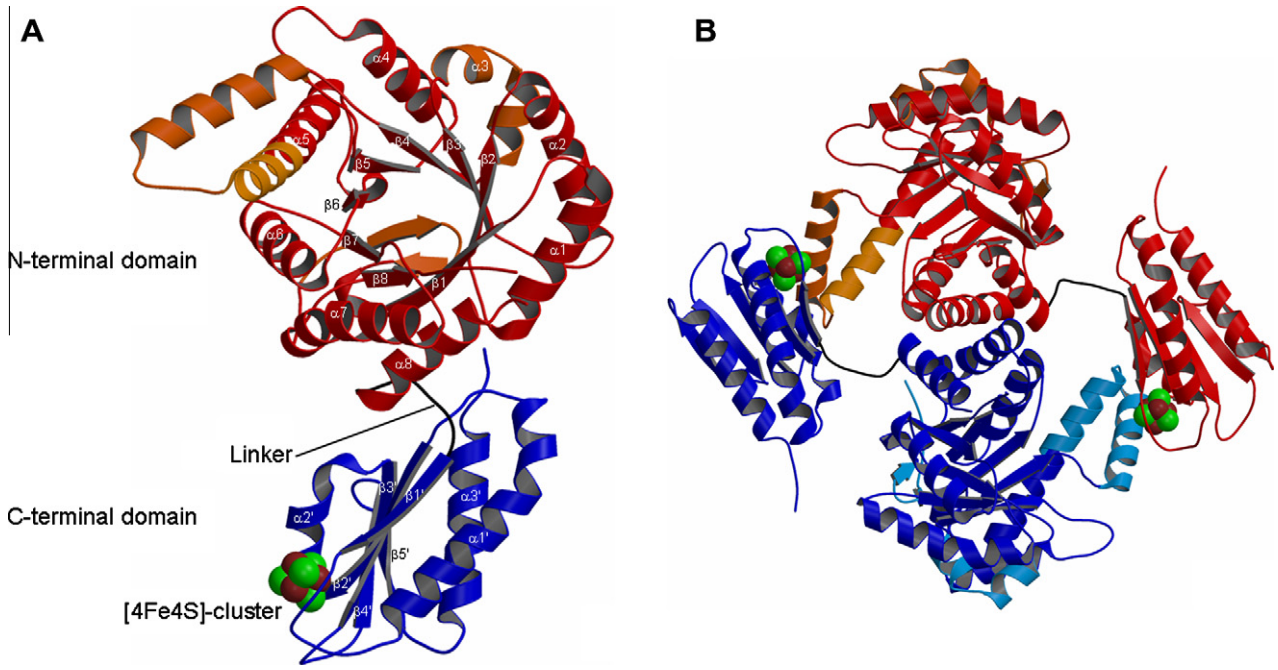

Fig. 2. Structure of GcpE. (A) The monomer is composed of a TIM barrel (in red and with marked secondary structures) and an open αβ barrel domain (blue; marked by dashed numbers). The irons and sulfurs of the [4Fe–4S] cluster are drawn as brown and green balls. (B) The dimer has a size of 95 × 80 × 40 Å^3. Its core built up of the TIM barrel domain of both subunits (red, blue) is linked to each of the open αβ domains by the helix-loop-helix protrusion and the polypeptide linker with a hole in between.

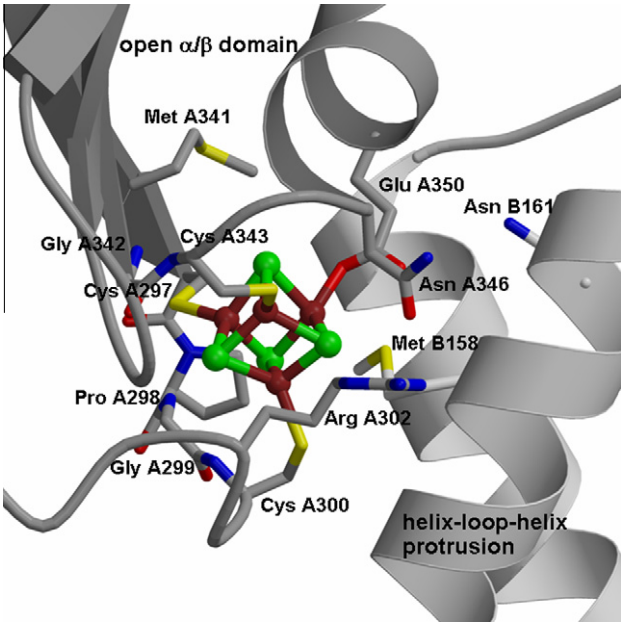

Fig. 3. Binding mode of the [4Fe–4S] cluster: The [4Fe–4S] cluster is ligated to the invariant CysA297, CysA300, CysA343 and GluA350. It is completely enveloped into the polypeptide matrix at the center of the monomer–monomer interface and thus inaccessible for the bulk solvent.

relatively small inter-subunit contact area and the low depth the cluster being buried. In the first interaction shell, the iron is ligated by three strictly conserved cysteine and, unexpectedly, by one glutamate side chains (Fig. 3). CysA297 protrudes from strand 1′, CysA300 from the following loop and CysA343 from the loop following strand 2′. The carboxylate side chain of the invariant GluA350 points from helix 2′ towards the [4Fe–4S] cluster and is surrounded by MetA341, AsnA346, MetB158 and AsnB161 the latter residues originating from the helix-loop-helix protrusion of the counter subunit. The carboxylate oxygen of GluA350, not ligated to the [4Fe–4S] cluster, might interact via a solvent molecule with AsnA346 and AsnB161. Glutamate/aspartate side chains are very rare ligands of [4Fe–4S] clusters but not unprecedented. An aspartate is found in light-independent protochlorophyllide reductase [24,25] and in some ferredoxins of thermophilic microorganisms [26]. In the second interaction shell, the [4Fe–4S] cluster non-covalently contacts several mostly invariant residues including ProA298, GlyA299, ArgA302, MetA341, GlyA342, AsnA346 and MetB158 (Fig. 2). The residues of the third shell are not in direct contact to the [4Fe–4S] cluster, but plug solvent-accessible gaps and thereby enhance the intersubunit interactions. For example, at one side of the interface, strands 1′ and helix 1′ and the first helix of the helix-loop-helix protrusion are linked together by hydrogen bonds between GlyA301 and ThrB155 and between ArgA302, AsnA346 and AspB159. At the other side lies a hydrophobic cluster consisting of ProA298, CysA300, TrpB146, LeuB154, MetB158 and ValB174. Despite their crucial function, the residues of the helix-loop-helix protrusion are, surprisingly, not significantly conserved.

3.3. Substrate binding and catalysis

Sequence comparison and protein surface analysis convincingly suggest in agreement with general structural principles the substrate binding site in front of the funnel-shaped C-terminal side of the TIM barrel (Fig. 2B). The funnel interior is coated by polar, predominantly positively charged residues which are highly conserved (Fig. 4). GlnA27, ValA85, ArgA141, HisA227 and SerA202 form the funnel bottom and ArgA56, AspA87, ArgA110, LysA204 and ArgA260 its sides (Fig. 4B). As the available space for binding the cyclic MEcPP is too large relative to the funnel size (due to its rapidly increasing diameter) and the positively charged side chains are widespread and conformationally variable, the exact position and orientation of the substrate is not reliably predictable. It appears plausible that the negatively charged diphosphate side of

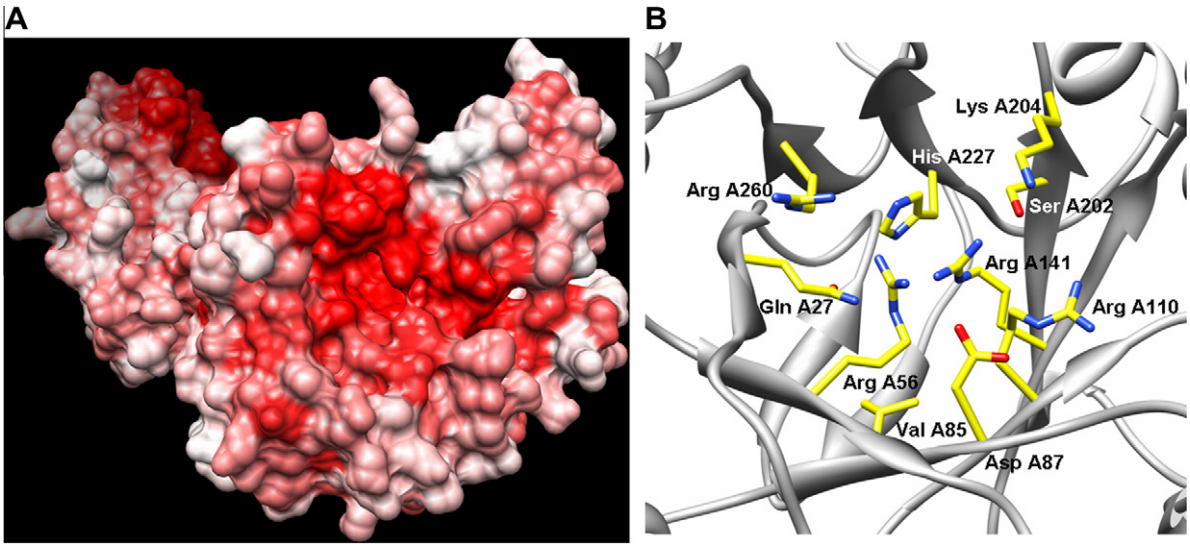

Fig. 4. Substrate-binding site: (A) The substrate MEcPP is embedded into the conserved funnel-shaped C-terminal side of the TIM barrel. The degree of conservation increases from white to red. (B) The interior of the funnel is coated by polar, mainly positively charged residues that are presumably responsible for substrate binding and activation.

the MEcPP ring points towards the funnel bottom and the catalytically active side towards the funnel entrance where the binding site of the [4Fe–4S] cluster in a closed state is expected (see below).

It became immediately obvious that the X-ray structure does not reflect a state of the reaction cycle from which the crucial catalytic steps proceed. In the current open structure the distance between the funnel bottom or a tentatively modeled substrate and the [4Fe–4S] cluster is ca. 25 or 20 Å, respectively, which is much too long for a direct participation of the [4Fe–4S] cluster in substrate binding and activation as proposed by recent EPR data [12,13]. The necessary reconciliation of these contradictory results requires a large-scale displacement of the open αβ relative to the TIM barrel domain of the counter subunit. We suggest that the complete αβ domain of the established open state moves as rigid body along the helix-loop-helix protrusion towards the TIM barrel opening and locks the funnel from the top (Supplementary Fig. 2). In the thereby created closed state the funnel interior is shielded from bulk solvent. During this process the iron-ligating Glu350 substantially changes its microenvironment and might be finally replaced as iron ligand by the substrate or an intermediate of the reaction.

Despite its limitation, the structure of the open state provides a first picture about the initial catalytic steps. After binding of the substrate into the open TIM barrel funnel (which is not possible in the closed state) epoxidation and ring opening of MEcPP [9,13] takes place prior to the redox process (Fig. 1). The intramolecular nucleophilic substitution reaction might be assisted by the invariant acid-base catalysts AspA87 and HisA227. We speculate that the drastic structural change from cyclic MEcPP to the open epoxide is propagated via strands 4, 5 and 6 to the helix-loop-helix protrusion and induces its dissociation from the counter subunit and the postulated open-to-close transition. In the closed state of GcpE, a docking site for the external electron donor is formed and the [4Fe–4S] cluster can be reduced. This proposal is compatible with EPR spectroscopic data [12,15] that showed reduction only in the presence of the substrate and with the suitability of the epoxide as substrate [27] which can obviously trigger an open-to-close transition. In addition, the break of the [4Fe–4S] cluster in the substrate-free open state by Ti(III) is prevented in the substrate-bound closed state [12] perhaps due to a shielding effect or to a shift of the redox potential in the new microenvironment of the [4Fe–4S] cluster.

4. Outlook

As the coordinates of *A. aeolicus* GcpE [18] were not available prior to manuscript submission we only add a brief structural comparison. As expected by an overall sequence identity of 41% the *A. aeolicus* and *T. thermophlus* GcpEs are highly related with rms values between the TIM barrel and open αβ domains of 1.6 and 2.2 Å, respectively. The major difference is related to an inter-domain rearrangement. In comparison to *T. thermophilus* GcpE, the open αβ domain of *A. aeolicus* GcpE is moved ca. 6 Å on the route postulated for the open-to-close transition towards the TIM barrel funnel opening of the counter subunit (Supplementary Fig. 2). For more profound investigations of the rigid-body domain movement, the catalytic mechanism and the exact substrate binding mode which is crucial for inhibitor design, the structure of the GcpE-substrate/product complex is indispensable.

Acknowledgements

This work was supported by the Max-Planck Society and the Else Kröner-Fresenius-Stiftung. We thank Hartmut Michel for continuous support and the staffs of PXII at the Swiss Light Source (Villigen) for help during data collection.

Appendix A. Supplementary data

Supplementary data associated with this article can be found, in the online version, at doi:10.1016/j.febslet.2010.12.012.

References

[1] Rohmer, M., Knani, M., Simonin, P., Sutter, B. and Sahm, H. (1993) Isoprenoid biosynthesis in bacteria: a novel pathway for the early steps leading to isopentenyl diphosphate. Biochem. J. 295 (2), 517–524.
[2] Eisenreich, W., Bacher, A., Arigoni, D. and Rohdich, F. (2004) Biosynthesis of isoprenoids via the non-mevalonate pathway. Cell Mol. Life Sci. 61, 1401–1426.
[3] Rohmer, M. (2008) From molecular fossils of bacterial hopanoids to the formation of isoprene units: discovery and elucidation of the methylerythritol phosphate pathway. Lipids 43, 1095–1107.
[4] Singh, N., Cheve, G., Avery, M.A. and McCurdy, C.R. (2007) Targeting the methyl erythritol phosphate (MEP) pathway for novel antimalarial, antibacterial and herbicidal drug discovery: inhibition of 1-deoxy-D-xylulose-5-phosphate reductoisomerase (DXR) enzyme. Curr. Pharm. Des. 13, 1161–1177.

[5] Wiesner, J., Reichenberg, A., Heinrich, S., Schlitzer, M. and Jomaa, H. (2008) The plastid-like organelle of apicomplexan parasites as drug target. Curr. Pharm. Des. 14, 855–871.
[6] Hecht, S., Eisenreich, W., Adam, P., Amslinger, S., Kis, K., Bacher, A., Arigoni, D. and Rohdich, F. (2001) Studies on the nonmevalonate pathway to terpenes: the role of the GcpE (IspG) protein. Proc. Natl. Acad. Sci. USA 98, 14837–14842.
[7] Kollas, A.K. et al. (2002) Functional characterization of GcpE, an essential enzyme of the non-mevalonate pathway of isoprenoid biosynthesis. FEBS Lett. 532, 432–436.
[8] Wolff, M., Seemann, M., Grosdemange-Billiard, C., Tritsch, D., Campos, N., Rodriguez-Concepcion, M., Boronat, A. and Rohmer, M. (2002) Isoprenoid biosynthesis via the methylerythritol phosphate pathway. (*E*)-4-Hydroxy-3-methylbut-2-enyl diphosphate: chemical synthesis and formation from methylerythritol cyclodiphosphate by a cell-free system from *Escherichia coli*. Tetrahedron Lett. 43, 2555–2559.
[9] Rohdich, F. et al. (2003) The deoxyxylulose phosphate pathway of isoprenoid biosynthesis: studies on the mechanisms of the reactions catalyzed by IspG and IspH protein. Proc. Natl. Acad. Sci. USA 100, 1586–1591.
[10] Seemann, M., Bui, B.T., Wolff, M., Tritsch, D., Campos, N., Boronat, A., Marquet, A. and Rohmer, M. (2002) Isoprenoid biosynthesis through the methylerythritol phosphate pathway: the (*E*)-4-hydroxy-3-methylbut-2-enyl diphosphate synthase (GcpE) is a [4Fe–4S] protein. Angew. Chem. Int. Ed. Engl. 41, 4337–4339.
[11] Brandt, W., Dessoy, M.A., Fulhorst, M., Gao, W., Zenk, M.H. and Wessjohann, L.A. (2004) A proposed mechanism for the reductive ring opening of the cyclodiphosphate MEcPP, a crucial transformation in the new DXP/MEP pathway to isoprenoids based on modeling studies and feeding experiments. ChemBioChem 5, 311–323.
[12] Xu, W., Lees, N.S., Adedeji, D., Wiesner, J., Jomaa, H., Hoffman, B.M. and Duin, E.C. (2010) Paramagnetic intermediates of (*E*)-4-hydroxy-3-methylbut-2-enyl diphosphate synthase (GcpE/IspG) under steady-state and pre-steady-state conditions. J. Am. Chem. Soc. 132, 14509–14520.
[13] Wang, W., Li, J., Wang, K., Huang, C., Zhang, Y. and Oldfield, E. (2010) Organometallic mechanism of action and inhibition of the 4Fe–4S isoprenoid biosynthesis protein GcpE (IspG). Proc. Natl. Acad. Sci. USA 107, 11189–11193.
[14] Seemann, M., Wegner, P., Schunemann, V., Bui, B.T., Wolff, M., Marquet, A., Trautwein, A.X. and Rohmer, M. (2005) Isoprenoid biosynthesis in chloroplasts via the methylerythritol phosphate pathway: the (*E*)-4-hydroxy-3-methylbut-2-enyl diphosphate synthase (GcpE) from Arabidopsis thaliana is a [4Fe–4S] protein. J. Biol. Inorg. Chem. 10, 131–137.
[15] Adedeji, D., Hernandez, H., Wiesner, J., Kohler, U., Jomaa, H. and Duin, E.C. (2007) Possible direct involvement of the active-site [4Fe–4S] cluster of the GcpE enzyme from *Thermus thermophilus* in the conversion of MEcPP. FEBS Lett. 581, 279–283.
[16] Seemann, M., Tse Sum Bui, B., Wolff, M., Miginiac-Maslow, M. and Rohmer, M. (2006) Isoprenoid biosynthesis in plant chloroplasts via the MEP pathway: direct thylakoid/ferredoxin-dependent photoreduction of GcpE/IspG. FEBS Lett. 580, 1547–1552.
[17] Seemann, M. and Rohmer, M. (2007) Isoprenoid biosynthesis via the methylerythritol phosphate pathway: GcpE and LytB, two novel iron–sulfur proteins. C R Chimie 10, 748–755.
[18] Lee, M., Grawert, T., Quitterer, F., Rohdich, F., Eppinger, J., Eisenreich, W., Bacher, A. and Groll, M. (2010) Biosynthesis of Isoprenoids: Crystal Structure of the [4Fe–4S] Cluster Protein IspG. J. Mol. Biol. 404, 600–610.
[19] Kabsch, W. (1993) Automatic processing of rotation diffraction data from crystals of initially unknown symmetry and cell constants. J. Appl. Cryst. 26, 795–800.
[20] Murshudov, G.N., Vagin, A.A. and Dodson, E.J. (1997) Refinement of macromolecular structures by the maximum-likelihood method. Acta Crystallogr. D Biol. Crystallogr. 53, 240–255.
[21] Kraulis, P.J. (1991) MOLSCRIPT: A program to produce both detailed and schematic plots of protein structures. J. Appl. Cryst. 24, 946–950.
[22] Pettersen, E.F., Goddard, T.D., Huang, C.C., Couch, G.S., Greenblatt, D.M., Meng, E.C. and Ferrin, T.E. (2004) UCSF Chimera–a visualization system for exploratory research and analysis. J. Comput. Chem. 25, 1605–1612.
[23] Holm, L. and Sander, C. (1993) Protein structure comparison by alignment of distance matrices. J. Mol. Biol. 233, 123–138.
[24] Muraki, N., Nomata, J., Ebata, K., Mizoguchi, T., Shiba, T., Tamiaki, H., Kurisu, G. and Fujita, Y. (2010) X-ray crystal structure of the light-independent protochlorophyllide reductase. Nature 465, 110–114.
[25] Brocker, M.J., Schomburg, S., Heinz, D.W., Jahn, D., Schubert, W.D. and Moser, J. (2010) Crystal structure of the nitrogenase-like dark operative protochlorophyllide oxidoreductase catalytic complex (ChlN/ChlB)2. J. Biol. Chem. 285, 27336–27345.
[26] Calzolai, L., Gorst, C.M., Zhao, Z.H., Teng, Q., Adams, M.W. and La Mar, G.N. (1995) 1H NMR investigation of the electronic and molecular structure of the four-iron cluster ferredoxin from the hyperthermophile *Pyrococcus furiosus*. Identification of Asp 14 as a cluster ligand in each of the four redox states. Biochemistry 34, 11373–11384.
[27] Nyland 2nd, R.L., Xiao, Y., Liu, P. and Freel Meyers, C.L. (2009) IspG converts an epoxide substrate analogue to (*E*)-4-hydroxy-3-methylbut-2-enyl diphosphate: implications for IspG catalysis in isoprenoid biosynthesis. J. Am. Chem. Soc. 131, 17734–17735.